Journal of Power Sources 239 (2013) 546–552

Contents lists available at SciVerse ScienceDirect

Journal of Power Sources

journal homepage: www.elsevier.com/locate/jpowsour

Aligned CdSe@ZnO flower-rod core–shell nanocable as photovoltaic application

Zhizhong Han [a], Liyuan Wei [a], Lele Tang [a,c], Chongqi Chen [a,b], Haibo Pan [a,c,*], Jianzhong Chen [a,**]

[a] College of Chemistry and Chemical Engineering, Fuzhou University, Fuzhou 350108, China
[b] National Engineering Research Center of Chemical Fertilizer Catalyst, Fuzhou 350002, China
[c] Fujian Key Lab of Medical Instrument and Pharmaceutical Technology, Fuzhou 350002, China

HIGHLIGHTS

- The CdSe@ZnO flower-rod core–shell nanocable arrays are used as photoanode.
- The photoanode of CdSe@ZnO nanocable exhibits higher photovoltaic performance.
- Ion exchange is a facile method to prepare the CdSe@ZnO nanocable.
- The CdSe-sensitized ZnO nanocables demonstrate a broad EQE in visible spectrum.

GRAPHICAL ABSTRACT

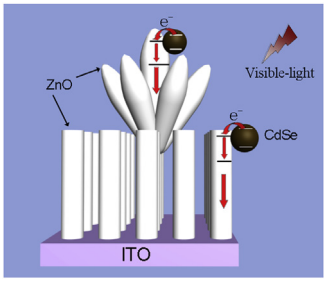

ARTICLE INFO

Article history:
Received 9 December 2012
Received in revised form
25 February 2013
Accepted 28 February 2013
Available online 14 March 2013

Keywords:
Solar cells
Quantum dots
ZnO
CdSe
Nanocable

ABSTRACT

The large bandgap of ZnO limits its application in photovoltaic devices, thus the semiconductor quantum dots (QDs), such as CdSe, is utilized to improve light-harvesting efficiency of solar cells. The CdSe@ZnO flower-rod core–shell nanocable arrays (CSZFRs) are prepared with a simple ion exchange method from aqueous solutions. The optical absorptions of the nanocable arrays can be controllably tuned to cover almost the entire visible spectrum (>750 nm) via quantum dots (QDs) sensitized attributed to the smaller band gap of CdSe. Moreover, a typical type II band alignment enhance the separation of photogenerated charge carriers, and reduce the electron–hole recombination within CSZFRs, demonstrated by the photoluminescence (PL) quenching after the formation of CSZFR hybrid structures. In addition, the CdSe-sensitized ZnO nanostructures demonstrate broad external quantum efficiency (EQE) in the spectrum from 300 to 740 nm. Therefore, the CSZFRs nanocable heterostruture exhibits a photovoltaic performance with a higher open-circuit photovoltage (−0.93 $V_{Ag/AgCl}$) and short-circuit photocurrent (1.00 mA cm^{-2}).

1. Introduction

The semiconductor metal oxides with large bandgap, such as TiO_2 and ZnO, have been found potential application in photovoltaic devices [1–7]. The large bandgap limits their photoresponse to only the UV region of the solar spectrum and restrain the efficient utilization of solar energy. For extension of the optical absorption into the visible-light region, one promising is coupling with organic dye or narrow band gap semiconductor quantum dots (QDs). Compared to organic dyes, QD sensitizers have several advantages, such as stability, higher light absorption [8], tailoring of optical absorption over a wider wavelength range [9], and high extinction coefficient, which is known to increase the overall power conversion efficiency of solar cells [10]. Therefore, such QD sensitized solar cells (QDSSCs) have attracted widespread attention and are now labeled third-generation or next-generation photovoltaic cells [11,12].

* Corresponding author. College of Chemistry and Chemical Engineering, Qishan Campus, Fuzhou University, Fuzhou, Fujian 350108, China. Tel./fax: +86 591 22866127.
** Corresponding author.
E-mail addresses: hbpan@fzu.edu.cn (H. Pan), j.z.chen@fzu.edu.cn (J. Chen).

0378-7753/$ – see front matter © 2013 Elsevier B.V. All rights reserved.
http://dx.doi.org/10.1016/j.jpowsour.2013.02.081

To enhance the efficiency of the QDSSCs, a three-dimensional (3D) semiconductor nanostructure matrix is generally utilized to work as a scaffold to hold the QDs dye, leading to an increase of the effective surface area of cell [13]. The nanomaterials also are work as photoelectrode and collect more photogenerated carriers. It have been reported that the aligned nanostructrue arrays can provide direct electrical pathways that ensure the rapid collection of carriers generated throughout the device [14]. The arrays also could increase light absorption attributed to scattering and trapping [15], which could be beneficial for photovoltaic applications. Moreover, it have been found that the core–shell nanocable architectures benefit carrier separation in the radial vs. the longer axial direction, with a carrier collection distance smaller or comparable to the minority carrier diffusion length [16–19]. In addition, ZnO has higher electron mobility than TiO_2 and is easy to grow in many different nanoscale forms, and the introduction of CdSe could extend the absorption edge to >700 nm [13]. Therefore, aligned ZnO flower-rod arrays were sensitized with CdSe quantum dots (CSZFRs) served as QDSCCs.

Many methods have been developed to sensitize semiconductor arrays with QDs, such as electrodeposition [20–22], successive ionic layer adsorption and reaction (SILAR) method [23,24], chemical bath deposition [25–27], ion exchange [28–30], and chemical vapor deposition (CVD) [31,32]. The feasibility of ion exchange process is due to the diversity of solubility product constant (Ksp). In our work, Ksp of ZnO (6.8×10^{-17}) is much larger than those of ZnSe (3.6×10^{-26}) and CdSe (6.31×10^{-36}). Thus, the formation of CdSe-sensitized ZnO is proposed to take place as following steps:

(i) In the Se and $NaBH_4$ solution, Se^{2-} ions are formed

$$Se + 2BH_4^- \rightarrow Se^{2-} + H_2 + 2BH_3$$

Then the surface of ZnO is converted to ZnSe by anion exchange

$$ZnO + H_2O + Se^{2-} \rightarrow ZnSe + 2OH^-$$

(ii) Since the smaller Ksp value of CdSe, CdSe is obtained via cation exchange

$$ZnSe + Cd^{2+} \rightarrow CdSe + Zn^{2+}$$

In this work, two steps are necessary to synthesis of CSZFRs as Fig. 1 show: (1) obtaining ZnO flower-rod arrays (ZFRs) via through a simple solution-based method and (2) decorating CdSe@ZFRs core–shell nanocable with ion exchange. The three samples exhibited different colors (Fig. 1), indicating that the process of ion exchange is successful. The nanocables based on indium doped tin oxide (ITO) are utilized as photoelectrodes, and the photovoltaic performance is improved by the sensitization of CdSe.

2. Experimental

2.1. Preparation of CSZFRs heterostructures on ITO

To prepare CSZFRs heterostructures, oriented ZFRs were firstly grown on ITO substrates (Heptachroma Solar Tech., 15 Ω sq^{-1}). Before the ZFRs growth, the substrates were cleaned by sonication in detergent, acetone, ethanol, and deionized water, and then dried in an oven. The substrates were then seeded by spin coating (1000 rpm, 50 s) with 5 mM zinc acetate dihydrate ($Zn(Ac)_2 \cdot 2H_2O$, 99%, Sino Chem. Reagent) in ethanol, followed by thermal decomposition at 300 °C for 20 min. The seeded substrates were placed in an aqueous solution containing 25 mM zinc nitrate hexahydrate ($Zn(NO_3)_2 \cdot 6H_2O$, 99%, Sino Chem. Reagent), 12.5 mM hexamethylenetetramine (HMTA, 99%, Sino Chem. Reagent), 5 mM polyethylenimine (PEI, 99%, Aladdin Reagent), and 0.35 M ammonium hydroxide ($NH_3 \cdot H_2O$, 25% ~ 28%, Sino Chem. Reagent) at 83–87 °C for 1–2 h. Finally, the as-prepared ZnO samples were dried in air and calcined at 450 °C for 0.5 h.

Aligned CSZFRs core–shell nanocable arrays were prepared by immersing the ZFRs arrays in a Se^{2-} ion solution (6.0 mM) prepared by reacting Se powder (Alfa Aesar) with $NaBH_4$ (Sino Chem. Reagent), and kept at 50 °C for 20–30 min. This process was repeated for two times to get a desirable thickness of ZnSe. The arrays of ZnO/ZnSe nanocables then reacted with a $Cd(NO_3)_2$ (Alfa Aesar) aqueous solution (0.1 M) at 90 °C for 8–10 h to replace Zn^{2+} by Cd^{2+} in the ZnSe shell. Finally, arrays of CSZFRs core–shell nanocables were prepared by annealing the samples in air at 400 °C for 30 min.

2.2. Material characterizations

Crystalline structures of CSZFRs were analyzed by powder X-ray diffraction (XRD, MiniFlexTMII, Japan). Surface morphologies of the samples across the entire substrate were characterized by field-emission scanning electron microscopy (FE-SEM, Hitachi S4800, Japan), while the transmission electron microscope (TEM, Tecnai G2 F20 S-TWIN, 200 kV, FEI, USA) was used to examine the morphology of CSZFRs. The diffuse reflectance spectra were measured on a Shimadzu UV-2500 UV–vis spectrophotometer. Raman spectrum was recorded by a confocal Raman microspectrometer (Renishaw, Great Britain) under the excitation of 785 nm diode laser and was collected in a range of 100–600 cm^{-1}. The photoluminescence (PL) spectra were recorded at room temperature employing a Cary Eclipase spectrophotometer (Varian, USA). For PL measurement, the ZFRs and CSZFRs were removed from the ITO. Then ZFRs and CSZFRs were dispersed in distilled water, and obtained at the same concentration for them. Except for FE-SEM, ZFRs and CSZFRs were scraped off from the ITO with a blade before characterizing.

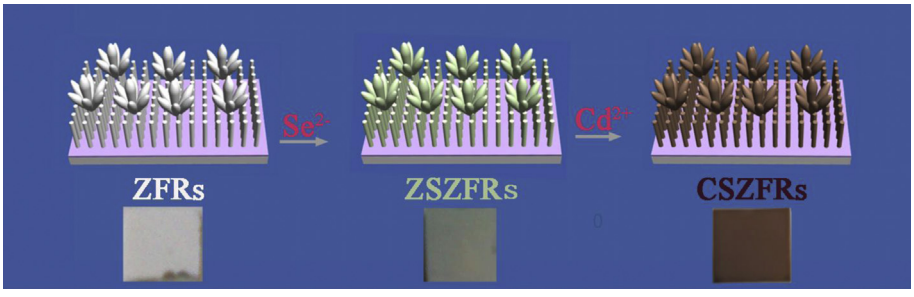

Fig. 1. Schematic illustration of the synthesis process of CSZFRs, and the optical images of the corresponding samples as denoted.

2.3. Photovoltaic measurements

The photovoltaic properties of the samples were performed with an electrochemical workstation (CHI 660D, CH Instrument Company, China). All electrochemical analyzes were executed using a conventional three-electrode system under a xenon lamp illumination. The working electrode was an as-prepared CSZFRs/ITO or ZFRs/ITO. A platinum wire and a saturated Ag/AgCl electrode were used as a counter and a reference electrode, respectively. The electrolyte solution was 0.1 M Na_2SO_4 aq solution containing 0.1 M Na_2S and 0.05 M Na_2SO_3. Photocurrent on and off cycles were measured using the same electrochemical workstation and the same illumination source. However, EQE of the devices was measured using an EQE system (model Oriel Merlin 70100) under AM 1.5G illumination with an intensity of 100 mW cm^{-2}, using polysulfide as electrolytes.

3. Results and discussion

As the Fig. 1 show, the sample color changed from white for the ZFRs to dark red for the CSZFRs, and corresponding absorption spectra of the samples are shown in Fig. 2. The band gaps of the ZFRs were estimated to be 3.11 eV from the onset of the absorption curves, which is red-shift compared to the bulk value, 3.2 eV. Compared with ZFRs, the absorption edge of CSZFRs shifted to 750 nm (1.66 eV), which suggests that the light absorption range of ZnO nanostructure arrays could be effectively extended to almost entire visible-light by the sensitization with CdSe shells. Furthermore, it also exhibits a red-shift due to pure CdSe nanocrystal as the Fig. 2 shown. The longer wavelength absorption in the cables may be because of the type II electronic structures of the core–shell heterojunctions, which enable an interface transition coupling a hole state in the shell (CdSe) with an electron state in the ZnO core [33]. However, the absorption edge of ZnSe sensitized ZnO array (ZSZFR) is close to pure ZFRs, matching its color in light yellow.

Fig. 3a displays the XRD patterns of the as-prepared samples. The pattern of CSZFRs demonstrates similar with that of ZFRs but its intensity is weaker, indicating that QDs cover the surface and restrain the growth of ZnO. Three distinct peaks at 31.8°, 34.4°, and 36.3° are observed in both patterns, which are representing (100), (002), and (101) ZnO crystal planes. These are assigned to pure wurtzite ZnO phase denoting $P6_3mc$ space group as cross-referenced to JCPDS 36-1451 card. However, the three peaks of CSZFRs show a systematic shift to lower 2θ compared with the pristine ZFRs. It is due to the increased lattice spacing resulting from the introduction with the larger Se atoms. The diffraction peaks of CdSe QDs are unclear, which is even the possibility that the QDs are too small to be detected by the X-ray diffractometer or the ZFRs are so big that its XRD peaks cover the QDs. To determine the crystal structure characteristics of the CdSe shells, ZnO cores of the cables were removed by etching in an acetic acid solution. As the inset of Fig. 3a show, three peaks located at 25.5°, 42.1°, and 49.9° are observed, which match well with the (111), (220), and (311) planes of cubic CdSe (JCPDF19-0191), respectively, indicating the formation of CdSe shells.

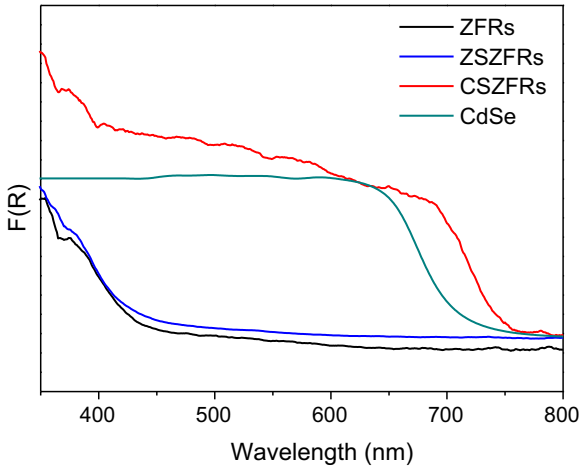

Fig. 2. UV–vis absorption spectra of ZFRs, ZSZFRs, CSZFRs, and pristine CdSe.

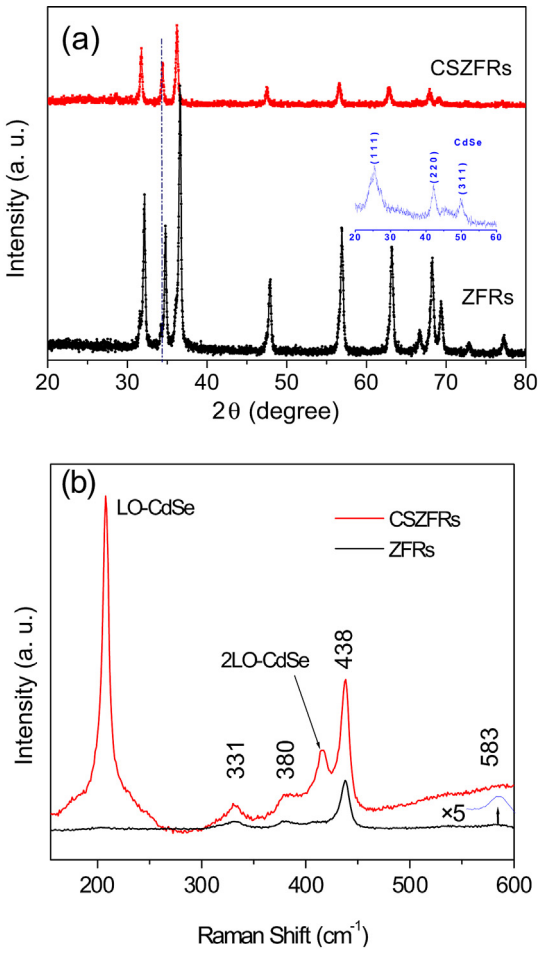

Fig. 3. (a) XRD patterns and (b) Raman spectra of ZFRs and CSZFRs. The inset shows the XRD pattern of CdSe shells after removing the ZnO cores via etching in an acetic acid solution.

The as-synthesized CSZFRs nanocable is further investigated with use of the confocal Raman studies as shown in Fig. 3b. The remarkable Raman mode at 438 cm^{-1} corresponds to the characteristic band of the wurtzite ZnO, which due to the ZnO nonpolar optical phonons E_2-(high) vibration mode. The peaks located at 331 and 380 cm^{-1} can be attributed to the $3E_{2H}$-E_{2L} mode of ZnO and the A_1 (TO) model, respectively [34]. Additionally, the E_1(LO) mode centered at 583 cm^{-1}, in which Zn atoms and O atoms have the same vibration direction to the neighbor lattices of the wurtzite ZnO, is observed in a magnified pattern of ZFRs [35]. Obviously, the results agree with the results of XRD that the as-synthesized ZFRs are the wurtzite structure. Carefully examination of the Fig. 3b, there is no remarkable shift of the Raman peak position between ZFRs and CSZFRs, while the intensities of CSZFRs nanocrystals are greatly enhanced compared with those of the ZnO cores. The

Raman peak centered at 207 cm^{-1} attaches to the first-order longitudinal optical phonon mode (LO), further confirming that the shell can be instead of CdSe.

Fig. 4 panels a and b show the field-emission scanning electron microscope (SEM) images of the as-grown ZFRs and CSZFRs on an ITO substrate. The ZnO nanorod array is displayed with a rod density of about 2.3×10^9 rods cm^{-2} and the average diameter of rod is 88 nm. Further, it is found that ZnO nanoflowers spread onto the nanorod arrays and cover up the film surface (inset of Fig. 4a). Compared with ZFRs, the CSZFRs have rougher surface, indicating

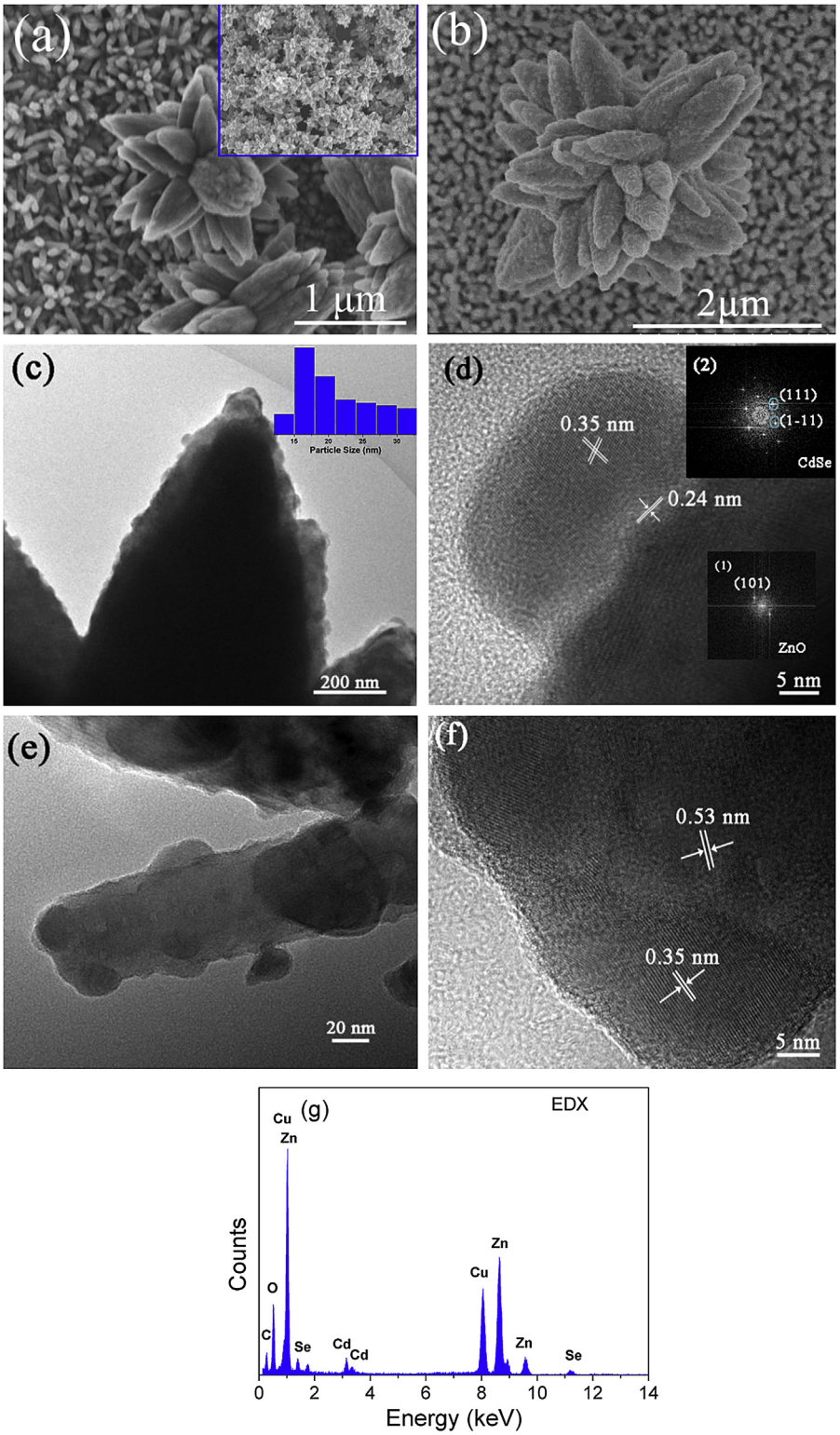

Fig. 4. (a) SEM images of ZFRs. (b) SEM images, (c, e) TEM images, (d, f) high-resolution TEM imags, and (g) EDS spectra of CSZFRs. The inset of (a) is an image with lower magnification. The inset of (c) displays the size distribution of CdSe particles. The insets of (d) show the FFT of (1) ZnO and (2) CdSe.

that the CdSe QDs cover very efficiently the ZnO substrate (Fig. 4b). The structures of the CSZFR nanocables are further illustrated by their TEM and high-resolution TEM (HRTEM) images in Fig. 4c, d, e, and f. Fig. 4c exhibits a TEM image of a CdSe/ZnO flower. Across the cable, the brightness profile shows a clear variation with a light-contrasted shell of 20–40 nm thick, which is close to ZnO core. The close contact between the core and shell favors electronic injection. And the average size of CdSe particles is about 19.6 nm via TEM analysis (inset of Fig. 4c). A high-resolution TEM image of the CdSe/ZnO flower nanocable is shown in Fig. 4d. The fringe spacing of 0.35 nm in the shell is attributed to the interplanar spacing of the {111} planes of cubic CdSe, while the fringe spacing of 0.24 nm in the boundary of core matches well to the interplanar spacing of the (101) plane of hexagonal ZnO. In addition, the fast Fourier transform (FFT) pattern (inset in Fig. 4d) also confirms this estimation. The TEM and HRTEM images of CdSe/ZnO rod arrays are shown in Fig. 4e and f. The fringe spacing of 0.53 nm in the core corresponds to the interspacing of the (001) planes of ZnO nanocrystal, while the fringe spacing in the shell is also 0.35 nm attributed to the interplanar spacing of the {111} planes of cubic CdSe. The energy dispersive X-ray (EDX) spectrum (Fig. 4g) was also carried out to analyze the component of the shell layer. As shown by the EDX spectrum, there are six major elements, i.e., Zn, O, Cd, Se, Cu, and C. Obviously, Zn and O peaks are corresponded to the ZFRs core, while the Cd and Se elements are derived from the CdSe shell. Whereas, Cu and C peaks results from the Cu grid and the supporting amorphous carbon film.

Room temperature PL measurements are widely used to characterize semiconductor nanoparticles which possess broad range of absorption, narrow emissions with high quantum yields, and size-tunable emission wavelength [36]. The room temperature PL spectra of both ZFRs and CSZFRs excited by the 350 nm laser are showed in Fig. 5. PL spectrum of ZnO usually is comprised of two emission bands: a near band edge (NBE) emission band and a visible emission peak [37]. The stronger NBE emission can be attributed to the direct radiative recombination of free excitons, whereas the broad visible emission is commonly assigned to the charge carrier relaxation via surface-related trap states. In visible region, there are two emission peaks: a narrow peak centered at 480 nm and a broad band around 600 nm. The emission band at 480 nm is attributed to recombination of isolated singly charged vacancy with photoexcited holes, and the latter is corresponding to the recombination of holes and double charged vacancy, which is created by capture of a hole by single charged vacancy in a depletion region [38]. Both of the PL spectra show a broad visible band, implying that the as-prepared ZFRs and CSZFRs nanostructures should have preferable electronic transport properties [31]. Moreover, the intensity of PL is found to be quenched heavily after the formation of CSZFR hybrid structures. The quenching of the NBE emissions for ZnO in the nanocable configuration is attributed to the band alignment between ZnO and CdSe, because a typical type II band alignment would enable the separation of photogenerated charge carriers, and thus reduce the electron–hole recombination within CSZFRs [20]. Therefore, the CSZFRs nanocables synthesized here can be used as photoelectrode for the fabrication of solar cells and improve photovoltaic performance.

To investigate the photo-induced behaviors and photoelectrochemical properties, the transient photocurrent responses of ZFRs and CSZFRs were carried out by potentiostatic (current density vs. time, J–t) measurements under intermittent illumination. Fig. 6a shows the J–t curve obtained from the photoelectrochemical cell under a 0 V vs. Ag/AgCl bias, which also exhibits that the photocurrent of the CdSe-sensitized ZFRs electrode (1.48 mA cm^{-2}) is much higher than that of the pristine ZnO heterostructure electrode (0.04 mA cm^{-2}) and CdSe-sensitized ZnO nanorod (CSZR) electrode (0.93 mA cm^{-2}) under visible light irradiation. The CSZFRs can absorb more solar energy due to the flower structures, leading to higher photocurrent compared with CSZRs. And it is not surprising that ZFRs exhibit very weak photocurrent because of their big band gaps. Moreover, under intermittent illumination, the

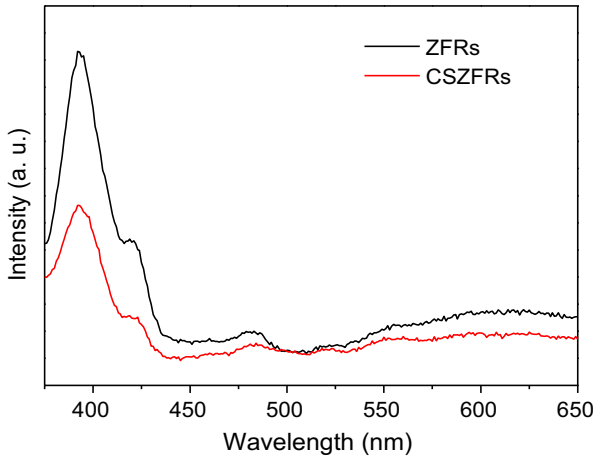

Fig. 5. Room temperature photoluminescence spectra of ZFRs and CSZFRs.

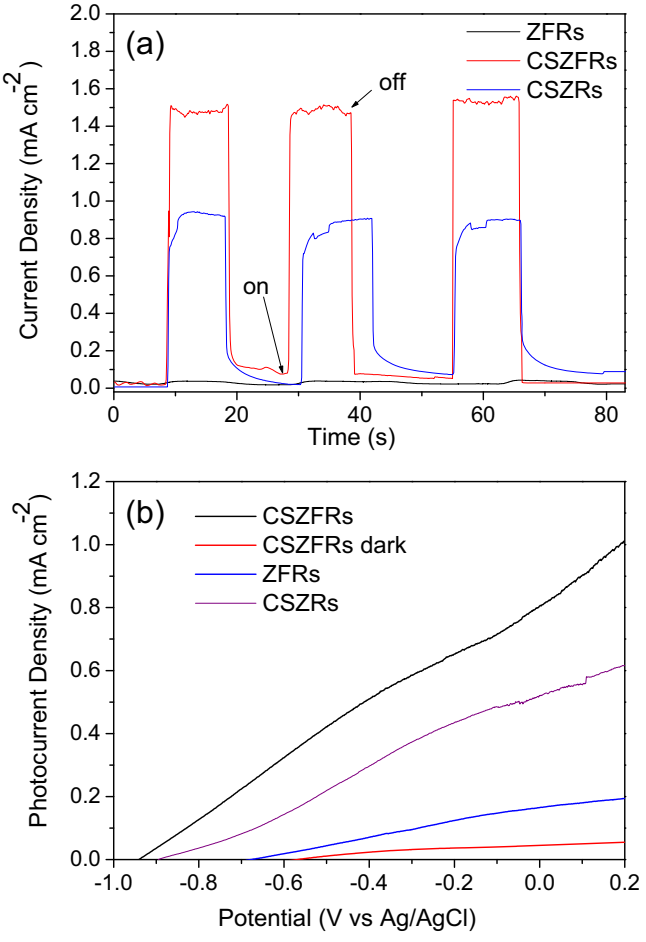

Fig. 6. (a) Photocurrent response of ZFRs, CSZRs and CSZFRs on ITO electrodes with on-off visible-light irradiation. (b) Photocurrent density for ZFRs, CSZRs and CSZFRs under visible light illumination.

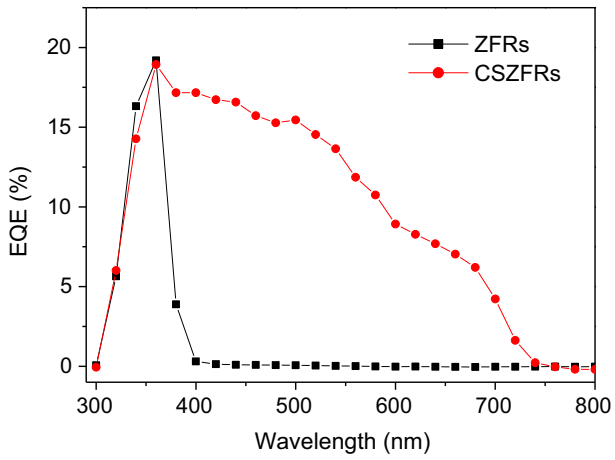

Fig. 7. A comparison between EQE spectra of ZFRs and CdSe-sensitized ZFRs.

photocurrent value of CSZFRs electrode drop to zero as soon as the illumination of light on the photoanode is stopped, and the photocurrent recover the original value once light is illuminated again on the sample, indicating that charge-transport properties are rapid [39].

Further, a comparison of the photocurrent between the plain ZFRs and CSZFRs was measured with a three electrode QDSSCs in an electrolyte solution containing Na_2S and Na_2SO_3. In fabrication of QDSSCs, a polysulfide electrolyte is suitable because the typical polyiodide (I^-/I_3^-) electrolyte, which has ideal kinetic properties in dye sensitized solar cells, is corrosive to semiconductor QDs [40]. Fig. 6b demonstrates the current density–voltage (J–V) curves measured from the plain ZFRs photoelectrode and the as-synthesized CSZFRs. The open-circuit photovoltage (V_{oc}) is −0.66 $V_{Ag/AgCl}$ for the pristine ZFRs electrode, but the deposition of CdSe nanoparticles on the ZnO arrays significantly increased V_{oc}, leading V_{oc} shifts to −0.93 $V_{Ag/AgCl}$ for the as-prepared CSZFRs electrode. The short-circuit photocurrent (J_{sc}) of the CdSe-sensitized ZFRs nanocables electrode (1.00 mA cm^{-2}) is about 5 times higher than that of the plain ZFRs electrode (0.19 mA cm^{-2}). The increasing J_{sc} is mainly due to the expanded absorption spectrum coverage of the CdSe@ZnO nanocable. Additionally, without light illumination, the V_{oc} is weakened to −0.57 $V_{Ag/AgCl}$ and J_{sc} is reduced to 0.05 mA cm^{-2}. It is also found that the CSZRs

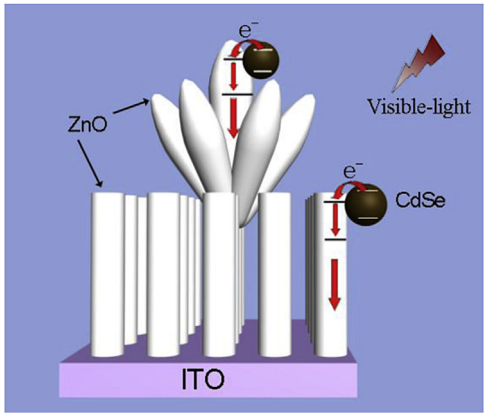

Scheme 1. Schematic of the electron transfer between CdSe and ZFRs. Electron injectes from excited CdSe shell into ZFRs core, and transfers to the ITO substrate along the aligned ZFRs.

show a large lower J_{sc} (0.62 mA cm^{-2}) than that of CSZFRs, but V_{oc} about −0.89 $V_{Ag/AgCl}$ is close to that of CSZFRs. This elucidates that the flower structures mainly improve the absorption of solar energy.

For analyzing quantitatively the photoactivity of the sensitized nanostructures, the external quantum efficiency (EQE) of the samples was investigated as a function of incident light wavelength. As presented in Fig. 7, the plain ZFRs only show quantum efficiency in the ultraviolet range (between 300 nm and 400 nm). However, a broad EQE in the spectrum from 300 to 740 nm can be observed for CdSe-sensitized ZFRs. Thus, the CSZFRs exhibit higher photoelectrichemical performance. This is owing to the broader light absorption range of CSZFRs than that of the bare ZFRs. Moreover, the CdSe shells as a passivation layer could protects the ZnO from etching by the electrolyte and restrain recombination of percolated electrons in the ZnO nanocrystal with the electrolyte [34].

The observed photoelectrochemical behavior for the CdSe-sensitized ZFRs may be attributed to the nanocable array configuration possessing uniform coverage. Moreover, it also due to the type II band alignment between ZnO and CdSe. As the Scheme 1 shown, both the valence-band maximum (VBM) and conduction-band minimum (CBM) of CdSe lie above those of ZnO. Upon visible light illumination, the photoinduced electrons can be easily transferred from QDs into the conduction band of ZnO core driven by the band alignment, generating photocurrent and enhancing the photoactivities.

4. Conclusions

In summary, the CdSe-sensitized ZnO flower-rod hybrid arrays were prepared with a simple ion exchange method from aqueous solutions. The deposited layers have been characterized by means of different techniques, paying particular attention to their morphology. The SEM images show that the CSZFRs have rougher surface compared with ZFRs, indicating that the CdSe QDs cover very efficiently the ZnO substrate. The TEM images demonstrate the CdSe QDs shell is close to the ZFRs core, which favors the electronic injection. Continuous tuning of optical absorption covering nearly the entire visible light region (>750 nm) has been achieved by CdSe sensitizing. The core–shell configuration, the type II band alignment, and the favorable absorption properties of CdSe contribute to high photovoltaic performance for the CSZFRs nanocables with a higher open-circuit photovoltage (−0.93 $V_{Ag/AgCl}$) and short-circuit photocurrent (1.00 mA cm^{-2}). In addition, the CdSe QDs can also significantly improve the quantum efficiency under visible light illumination. The flexibility of tailoring various materials via the simple ion exchange approach makes it a very promising synthetic method for preparation of ZnO-based heterostructures with custom-designed properties for different applications.

Acknowledgments

The authors gratefully acknowledge the financial support from National Natural Science Foundation of China (91022025, 51072036, and 21201035), and Fujian Natural Science Foundation (2012J01204). Thank institute of biomedical and pharmaceutical technology, Fuzhou University, for material characterization.

References

[1] K. Lee, S. Park, M.J. Ko, K. Kim, Nam-Gyu Park, Nat. Mater. 8 (2009) 665.
[2] C. Wang, Z. Jiang, L. Wei, Y. Chen, J. Jiao, M. Eastman, H. Liu, Nano Energy 1 (2012) 440.
[3] J.A. Anta, E. Guillén, R. T.-Zaera, J. Phys. Chem. C 116 (2012) 11413.
[4] T. Bora, H.H. Kyaw, J. Dutta, Electrochim. Acta 68 (2012) 141.

[5] C.K. Xu, J.M. Wu, U.V. Desai, D. Gao, J. Am, Chem. Soc. 133 (2011) 8122.
[6] H.M. Chen, C.K. Chen, C.C. Lin, R.-S. Liu, H. Yang, W.-S. Chang, K.-H. Chen, T.-S. Chan, J.-F. Lee, D.P. Tsai, J. Phys. Chem. C 115 (2011) 21971.
[7] P. Sudhagar, T. Song, D.H. Lee, I. M.-Seró, J. Bisquert, M. Laudenslager, W.M. Sigmund, W.I. Park, U. Paik, Y.S. Kang, J. Phys. Chem. Lett. 2 (2011) 1984.
[8] G. Hodes, J. Phys. Chem. C 112 (2008) 17778.
[9] A. Kongkanand, K. Tvrdy, K. Takechi, M. Kuno, P.V. Kamat, J. Am. Chem. Soc. 130 (2008) 4007.
[10] S.S. Mali, S.K. Desai, S.S. Kalagi, C.A. Betty, P.N. Bhosale, R.S. Devan, Y.R. Ma, P.S. Patil, Dolton Trans. 41 (2012) 6130.
[11] A.J. Nozik, M.C. Beard, J.M. Luther, M. Law, R.J. Ellingson, J.C. Johnson, Chem. Rev. 110 (2010) 6873.
[12] S. Rühle, M. Shalom, A. Zaban, ChemPhysChem 11 (2010) 2290.
[13] Z. Lu, J. Xu, X. Xie, H. Wang, C. Wang, S.-Y. Kwok, T. Wong, H.L. Kwong, I. Bello, C.-S. Lee, S.-T. Lee, W. Zhang, J. Phys. Chem. C 116 (2012) 2656.
[14] M. Seol, H. Kim, Y. Tak, K. Yong, Chem. Commun 46 (2010) 5521.
[15] Y.-J. Lee, D.S. Ruby, D.W. Peters, B.B. McKenzie, J.W.P. Hsu, Nano Lett. 8 (2008) 1501.
[16] N.S. Lewis, Science 315 (2007) 798.
[17] Y. Zhang, L.-W. Wang, A. Mascarenhas, Nano Lett. 7 (2007) 1264.
[18] B. Tian, X. Zheng, T.J. Kempa, Y. Fang, N. Yu, G. Yu, J. Huang, C.M. Lieber, Nature 449 (2007) 885.
[19] B. Tian, T.J. Kempa, C.M. Lieber, Chem. Soc. Rev. 38 (2009) 16.
[20] X. Wang, H. Zhu, Y. Xu, H. Wang, Y. Tao, S. Hark, X. Xiao, Q. Li, ACS Nano 4 (2010) 3302.
[21] Z. Shao, W. Zhu, Z. Li, Q. Yang, G. Wang, J. Phys. Chem. C 116 (2012) 2438.
[22] C.Z. Yao, B.H. Wei, L.X. Meng, H. Li, Q.J. Gong, H. Sun, H.X. Ma, X.H. Hu, J. Power Sources 207 (2012) 222.
[23] N. Guijarro, T. L.-Villarreal, Q. Shen, T. Toyoda, R. Gómez, J. Phys. Chem. C 114 (2010) 21928.
[24] J. Ryu, S.H. Lee, D.H. Nam, C.B. Park, Adv. Mater 23 (2011) 1883.
[25] T. Zeng, H. Tao, X. Sui, X. Zhou, X. Zhao, Chem. Phys. Lett. 508 (2011) 130.
[26] Z.X. Li, Y.L. Xie, H. Xu, T.M. Wang, Z.G. Xu, H.L. Zhang, J. Photochem. Photobio. A 224 (2011) 25.
[27] Y. Xie, S.H. Yoo, C. Chen, S.O. Cho, Mater. Sci. Eng. B 177 (2012) 106.
[28] S.V. Chong, N. Suresh, J. Xia, N. A.-Salim, H. Idriss, J. Phys. Chem. C 111 (2007) 10389.
[29] D. Kelly, A. Singh, C.A. Barrett, C. O'Sullivan, C. Coughlan, F.R. Laffir, C. O'Dwyer, K.M. Ryan, Nanoscale 3 (2011) 4580.
[30] Y.F. Zhu, G.H. Zhou, H.Y. Ding, A.H. Liu, Y.B. Lin, Y.W. Dong, Superlattice Microst 50 (2011) 549.
[31] H. Li, C. Cheng, X. Li, J. Liu, C. Guan, Y. Yan Tay, H.J. Fan, J. Phys. Chem. C 116 (2012) 3802.
[32] Y. Myung, D.M. Jang, T.K. Sung, Y.J. Sohn, G.B. Jung, Y.J. Cho, H.S. Kim, J. Park, ACS Nano 4 (2010) 3789.
[33] J. Xu, X. Yang, H.K. Wang, X. Chen, C.Y. Luan, Z.X. Xu, Z.Z. Lu, V.A.L. Roy, W.J. Zhang, C.-S. Lee, Nano Lett. 11 (2011) 4138.
[34] X.F. Zhou, Z.L. Hu, Y.Q. Fan, S. Chen, W.P. Ding, N.P. Xu, J. Phys. Chem. C 112 (2008) 11722.
[35] T.C. Damen, S.P.S. Porto, B. Tell, Phys. Rev. 142 (1966) 570.
[36] N. Udawatte, M. Lee, J. Kim, D. Lee, ACS Appl. Mater. Interfaces 3 (2011) 4531.
[37] B.J. Niu, L.L. Wu, W. Tang, X.T. Zhang, Q.G. Meng, CrystEngComm 13 (2011) 3678.
[38] S. Sarkar, A. Makhal, T. Bora, S. Baruah, J. Duttab, S.K. Palz, Phys. Chem. Chem. Phys. 13 (2011) 12488.
[39] S. Banerjee, S.K. Mohapatra, P.P. Das, M. Misra, Chem. Mater. 20 (2008) 6784.
[40] Y.L. Lee, C.H. Chang, J. Power Sources 185 (2008) 584.